1D Co-Pi Modified $BiVO_4$/ZnO Junction Cascade for Efficient Photoelectrochemical Water Cleavage

*Savio J. A. Moniz, Jun Zhu, and Junwang Tang**

The most important factors dominating solar hydrogen synthesis efficiency include light absorption, charge separation and transport, and surface chemical reactions (charge utilization). In order to tackle these factors, an ordered 1D junction cascade photoelectrode for water splitting, grown via a simple low-cost solution-based process and consisting of nanoparticulate $BiVO_4$ on 1D ZnO rods with cobalt phosphate (Co-Pi) on the surface is synthesized. Flat-band measurements reveal the feasibility of charge transfer from $BiVO_4$ to ZnO, supported by PL measurements and photocurrent observation in the presence of an efficient hole scavenger, which demonstrate that quenching of luminescence of $BiVO_4$ and enhanced current are caused by electron transfer from $BiVO_4$ to ZnO. A dramatic cathodic shift in onset potential under both visible and full arc irradiation, coupled with a 12-fold increase in photocurrent (ca. 3 mA cm^{-2}) are observed compared to $BiVO_4$, resulting in ≈47% IPCE at 410 nm (4% for $BiVO_4$) with high solar energy conversion efficiency (0.88%). The reasons for these enhancements stem from enhanced light absorption and trapping, in situ rectifying electron transfer from $BiVO_4$ to ZnO, hole transfer to Co-Pi for water oxidation, and facilitating electron transport along 1D ZnO.

1. Introduction

There has been intense research into the development of visible-light active semiconductor photocatalysts for solar energy conversion, in particular, for oxidation and reduction of water into molecular oxygen and hydrogen, which can be used as a clean, renewable fuel source. There are several challenges that need to be addressed before the implementation of such a process. The semiconductor must possess a suitable band-gap, preferably in the visible range, with a conduction band more negative than 0 V and the valence band more positive than 1.23 V.[1] It is widely accepted that the most important factors dominating solar hydrogen synthesis efficiency include: i) light absorption; ii) charge separation and transport; and iii) surface chemical reactions (charge utilization).[2,3] Numerous materials have been reported to split water under UV and/or visible irradiation via a photoelectrochemical process; the most widely reported being TiO_2, $SrTiO_3$ and $KTaO_3$,[4] as well as Fe_2O_3,[5] WO_3[6,7] and $BiVO_4$.[8,9] However the current solar to fuel conversion efficiency is still moderate. A new material strategy therefore is required to enhance the energy conversion efficiency, such as via manipulating the aforementioned important factors. Suppression of charge recombination is one of the key solutions, which can be attempted in a number of ways: i) the use of scavengers (sacrificial solutions), which can remove either holes or electrons in the system so that only one half of the water splitting reaction can be studied in isolation (either reduction or oxidation); ii) variation of the morphology of the photocatalyst, which has been shown to improve photocatalytic activity due to the increase in surface area and the shortening of charge carrier diffusion pathways to the surface; and iii) the most promising way is to create a heterojunction, whereby charge carriers are generated in one photocatalyst and subsequently vectorially transferred to the other material, mimicking natural photosynthesis. Beyond this, the separated charge transport also needs to be enhanced to improve the energy conversion efficiency.

Here, we attempted to design a special morphology of heterojunction to tackle the above-mentioned three dominating factors in order to achieve efficient photoelectrochemical water splitting to molecular H_2 and O_2. In other words, an ordered 1D morphology will be used to enhance light absorption by light trapping effect;[10,11] a heterojunction is used for in situ rectifying charge transfer and separation as well as the appropriate charge acceptor will be selected to further facilitate the transport of separated charges; finally an efficient co-catalyst is utilized to accelerate the surface reactions, as indicated in **Scheme 1** composed of a junction cascade.

Monoclinic $BiVO_4$, as a well-known, stable n-type semiconductor with a direct band-gap of approximately 2.4 eV, was selected as the robust light absorber due to its reported extremely high visible driven photocatalytic activity for oxygen evolution from aqueous $AgNO_3$ solution in a suspension system.[12] There are, however, a number of limiting factors which act to reduce the energy conversion efficiency of the

Dr. S. J. A. Moniz, Dr. J. Tang
Department of Chemical Engineering
University College London
Torrington Place, London WC1E 7JE, UK
E-mail: Junwang.tang@ucl.ac.uk
Dr. J. Zhu
Key Lab of Novel Thin Film Solar Cells
Institute of Plasma Physics
Chinese Academy of Sciences
P.O. Box 1126, Hefei 230031, China

DOI: 10.1002/aenm.201301590

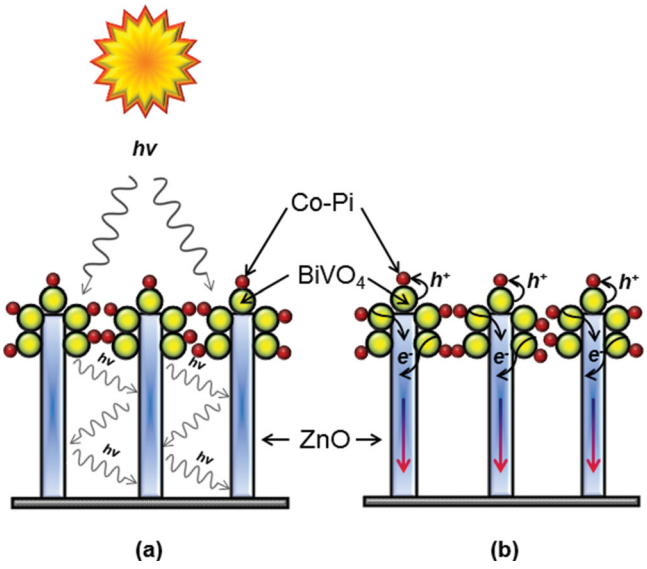

Scheme 1. Design strategy of a $BiVO_4$/ZnO heterojunction, involving a) increased light absorption and charge generation in both $BiVO_4$ and ZnO in conjunction with light trapping effect of the nanorods and b) electron injection into ZnO nanorods followed by prompt electron transport along ZnO nanorods and simultaneous hole transfer to Co-Pi for efficient water oxidation.

material, which include, but are not limited to: i) significant recombination of photogenerated electron–hole pairs, ii) poor electron mobility, and iii) slow hole transfer kinetics for water oxidation.[13] A few examples have recently been reported to improve efficiency of $BiVO_4$ by a single heterojunction, e.g., $BiVO_4$ with WO_3[14] or SnO_2/WO_3[15] to suppress charge-carrier recombination. However WO_3 has the similar issue of poor electron mobility which limits the electron migration in the photoanode to the counter electrode and influences hole transfer kinetics in $BiVO_4$. Very recently, Kudo successfully carried out pure water splitting using a CoO-$BiVO_4$ p-n junction photoanode with a Pt counter electrode, achieving a relatively high solar energy conversion efficiency of 0.04%.[16] In addition, surface modification has also been employed to improve photocatalytic performance of $BiVO_4$, most notably through the use of oxygen evolution catalysts such as cobalt complexes (Co-Pi)[17] or FeOOH.[18,19] Very recently a Co-Pi/homojunction W:$BiVO_4$ electrode coupled to a Si solar cell in tandem configuration achieved photocurrents between 3–4 mA cm^{-2} at 1.23V vs RHE.[20] However the inherent problems of poor electron mobility and conductivity in $BiVO_4$ still remain.[21]

In order to solve the problems existing in the above-mentioned examples, we chose one-dimensional ZnO with an extremely high intrinsic electron mobility as the electron acceptor to facilitate charge injection and transport. The flat-band potentials (E_{fb}) of both $BiVO_4$ and ZnO lie within a very broad range of values; for $BiVO_4$ it has been estimated to lie between approximately –0.7 and –0.3 V (vs Ag/AgCl, pH 5.8 – 7)[14,22–24] and for ZnO between –0.29 V and +0.2 V (vs Ag/AgCl, pH 7.4),[25] suggesting that electron transfer from $BiVO_4$ to ZnO is possible, thus resulting in in situ separated electrons and holes by the heterojunction. The use of ZnO in the form of nanorods has also been demonstrated to improve electron transport due to their internal electric field in other applications.[26] Furthermore, the 1D structure, in theory, can substantially trap photons, which should increase light absorption compared with a flat surface. Finally, addition of an earth abundant cobalt phosphate complex upon the surface of $BiVO_4$ forms a junction cascade Co-Pi/$BiVO_4$/ZnO, in which the complex Co-Pi acts as a hole acceptor and catalytic site to speed up water oxidation. This new design strategy, comprised of a bi-junction, represents the first successful example of $BiVO_4$-based junction cascade photoelectrode for water splitting, and has been fully investigated and the performance optimized in the paper. The stability of the novel structure was also discussed.

2. Results and Discussion

Bare $BiVO_4$, ZnO and 1D $BiVO_4$/ZnO heterojunction films were grown directly onto FTO-coated glass substrates using a combination of solution-based hydrolysis-condensation synthesis and spray deposition (see Experimental Section). The X-ray diffraction (XRD) patterns for ZnO, $BiVO_4$ and $BiVO_4$/ZnO are displayed in **Figure 1**a. XRD confirmed the presence of ZnO exhibiting a Wurtzite structure with strong preferred orientation; the growth direction of the nanorods was assigned to the <0002> direction as expected for the nanorod morphology of ZnO grown from acetate seed crystals, which results in *c*-axis texturing.[27,28] The as-deposited $BiVO_4$ films grown via spray deposition at 200 °C were of a dark-yellow to brown appearance, and X-ray diffraction analysis revealed no crystalline phase(s) at this temperature (not shown). Subsequent heat treatment in air at 450 °C for 3 h is necessary which yields pure monoclinic $BiVO_4$ possessing the Scheelite structure. The heterojunction $BiVO_4$/ZnO films were grown through directly spraying the Bi-V solution onto the ZnO nanorods followed by heat treatment at 450 °C.

The UV-vis absorption spectra of $BiVO_4$, ZnO nanorods, and $BiVO_4$/ZnO heterojunction are shown in Figure 1b. The band-gap (E_g) of a semiconductor could be inferred from its UV-vis spectra using the following equation:

$$(\alpha h\upsilon)^n = A(h\upsilon - E_g) \quad (1)$$

where α is the absorption coefficient, $h\upsilon$ is the energy of photon, n represents the index which depends on the electronic transition of the semiconductor (for direct band-gap semiconductors $BiVO_4$ and ZnO, $n = 2$). In addition, A is a proportionality constant related to the material. The band-gap energy was obtained from the intercept of the tangent line in the plot of $(\alpha h\upsilon)^2$ versus energy, and the value was determined to be ≈2.3 eV for $BiVO_4$ and ≈3.2 eV for ZnO (see Supporting Information Figure S1a). The 1D $BiVO_4$/ZnO heterojunction displayed much higher absorption within the visible region of the spectrum (Figure 1b), with the edge at ≈490 nm corresponding to $BiVO_4$ and the edge at ≈390 nm corresponding to ZnO nanorods. Similar increase caused by light trapping has been observed on bare ZnO nanowires compared to flat ZnO films,[10] as well as on CdTe/ZnO nanowire arrays.[11] On the other hand, formation of mid-gap states caused by, amongst other factors, the defect chemistry of ZnO, could lead to the formation of broad mid-gap states and show an enhanced visible band absorption. However,

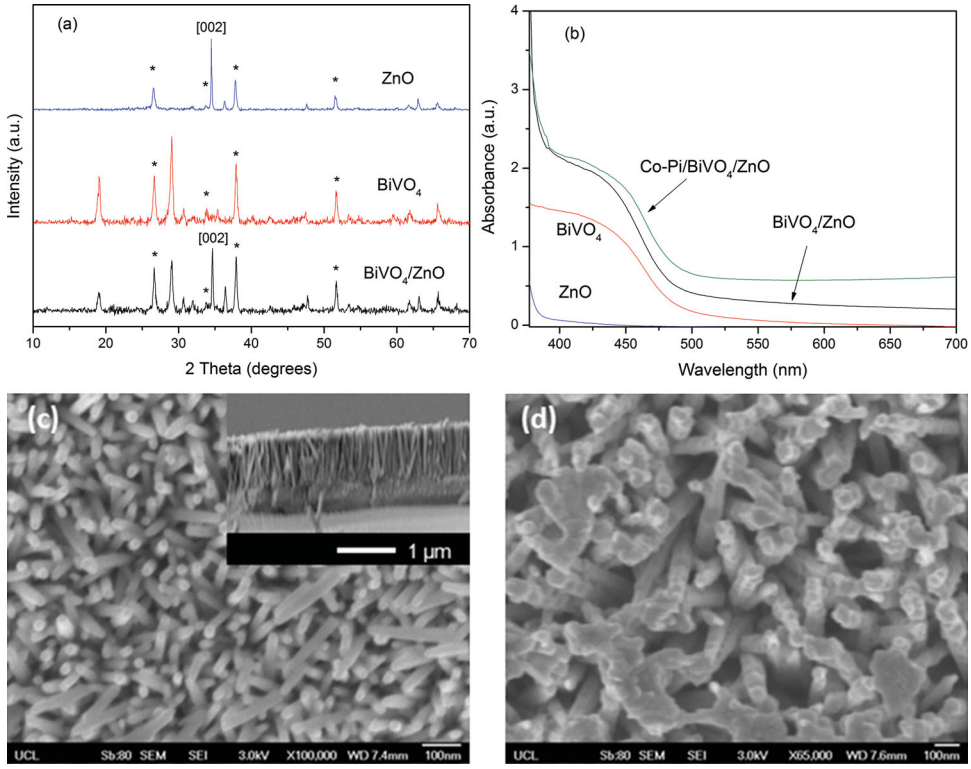

Figure 1. a) XRD patterns of ZnO, $BiVO_4$ and $BiVO_4$/ZnO. Asterisks (*) correspond to diffraction peaks arising from the fluorine-doped tin oxide (FTO) substrate. b) UV-vis absorption spectra of $BiVO_4$, ZnO, 1D $BiVO_4$/ZnO and Co-Pi/$BiVO_4$/ZnO photoelectrodes. c) SEM images of ZnO nanorods; the insert shows a cross-section image of ZnO nanorods. d) Top-down SEM image of a 1D $BiVO_4$/ZnO heterojunction, indicating a compact contact between 1D ZnO and $BiVO_4$.

the junction shows very similar band-gap absorption (similar profile) to $BiVO_4$ except enhanced intensity in the visible region. Therefore the obvious enhanced absorption in the visible region (>400 nm) is attributed to the light-trapping effect as expected due to a 1D aligned morphology of the heterojunction. A somewhat red-shift in the spectrum might be due to the formation of shallow levels within the band gap as a result of the presence of impurity atoms in the lattice and/or strong disturbances of local symmetry.[29] The Raman spectrum of the 1D $BiVO_4$/ZnO heterojunction (Supporting Information Figure S1b) revealed a strong peak at 440 nm, consistent with the high-E_2 vibration of wurtzite ZnO,[30] whilst the other strong peak at ≈823 nm corresponds to the ν_1 symmetric stretching mode of monoclinic $BiVO_4$[31] and provides further evidence of the incorporation of both materials within the same photoanode.

The top-down and side-on SEM image of ZnO nanorods are displayed in Figure 1c. Growth of vertically aligned ordered ZnO nanorods for 4 h via hydrolysis-condensation synthesis results in very homogeneous nanorods with a length of 900 nm and a diameter of 70 nm.[28] Top-down SEM images of bare $BiVO_4$ after heat treatment reveals a dense morphology of good substrate coverage and uniformity (see Supporting Information Figure S2a). The top-down SEM image of the heterojunction $BiVO_4$/ZnO film (Figure 1d) reveals that the spray deposition procedure mainly introduced $BiVO_4$ agglomerations at the tops of the nanorods which can, as expected, facilitate charge separation at the interface of $BiVO_4$ and ZnO. The side view of the junction confirms that the coating procedure of $BiVO_4$ did not change the length, nor the ordered morphology of the ZnO substrate (see Supporting Information Figure S2b), which also reveals the major $BiVO_4$ coating to be on the top surface of the vertically aligned nanorods to form the intimate contact, which is important for the proposed fast charge transfer between them.

Impedance measurements conducted on $BiVO_4$, and ZnO electrodes in 0.2 M Na_2SO_4 electrolyte in the dark allowed the construction of Mott-Schottky plots from which the flat-band potentials (E_{fb}) of the two materials were measured. **Figure 2**a shows the Mott–Schottky plots of $BiVO_4$ and ZnO electrodes measured at 1 kHz. Using our device we observed poor reproducibility at higher frequencies due to the frequency dependence of charge carrier density and mobility, however in all cases the intercepts for E_{fb} were very close in agreement with each other. The E_{fb} of the $BiVO_4$ electrode was estimated to be –0.53 V (*vs* Ag/AgCl at pH 6.5) or +0.05 V (vs RHE) and is very similar to the value measured at 1000 Hz by Zou et al. for their undoped $BiVO_4$ electrodes in 0.5 M Na_2SO_4 (pH 6.5).[32] E_{fb} for ZnO nanorods was estimated as –0.33 V (vs Ag/AgCl at pH 6.5) or +0.25 V (vs RHE). The difference in the E_{fb} values for $BiVO_4$ and ZnO measured under identical conditions in our laboratory indicate that electron transfer in principal from $BiVO_4$ to ZnO is feasible as E_{fb} is considered to be located just under the conduction band of n-type semiconductors.[23] Even so, there are many values reported in the literature for the E_{fb} of $BiVO_4$, which tend to be in the range of –0.7 to –0.3 V (vs Ag/AgCl, pH 5.8– 7).[22–24] Similarly, for ZnO nanorods, values for E_{fb} have

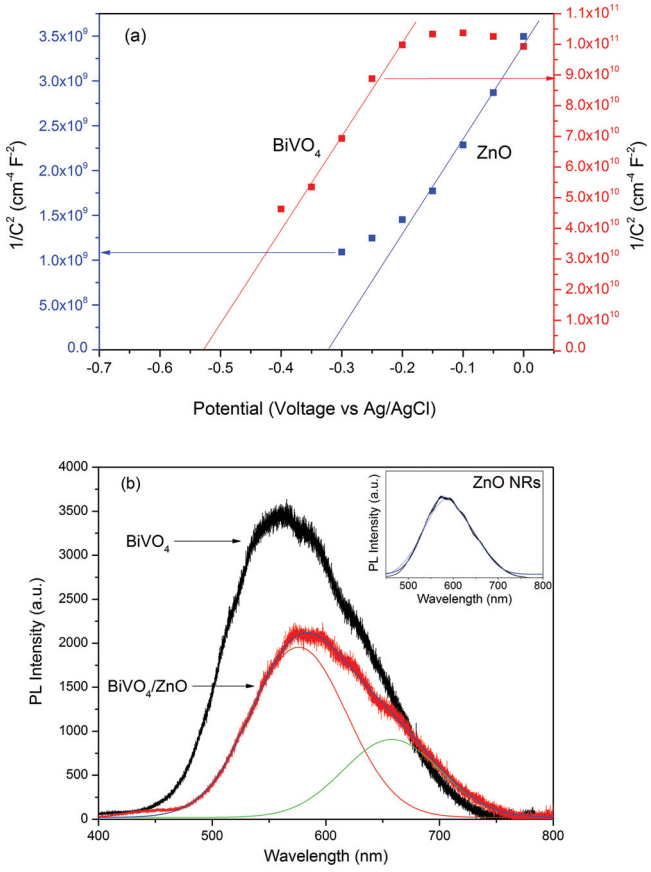

Figure 2. a) Mott-Schottky plots for $BiVO_4$ nanoparticulates and ZnO nanorods measured in 0.2 M Na_2SO_4 (pH 6.5) at 1 kHz. (b) PL spectrum of bare $BiVO_4$ and 1D $BiVO_4$/ZnO heterojunction excited at a laser wavelength of 325 nm. The smooth red and green lines show the curve fitting for the individual component materials. The inset figure displays the PL spectrum of bare ZnO nanorods. Both indicate efficient charge rectifying effect by the ordered junction with the PL spectra decreased by nearly 50%.

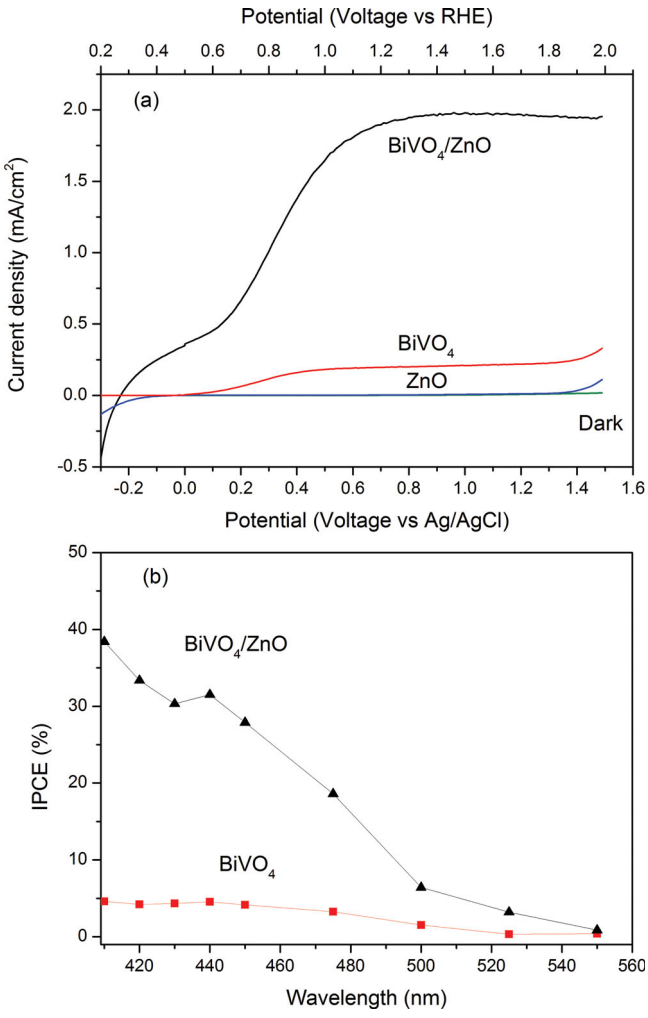

Figure 3. a) Current vs potential curve of a 300 nm $BiVO_4$/900 nm ZnO heterojunction film in a 0.2 M Na_2SO_4 solution (pH 6.5), under visible light ($\lambda > 420$ nm) with AM 1.5G illumination. b) IPCE spectra for bare $BiVO_4$ and single junction $BiVO_4$/ZnO measured at 1.2 V vs RHE.

been reported in the range of +0.2 V to –0.29 V (vs Ag/AgCl, pH 7.4) due to the fact that these values, as stated previously, are strongly dependent upon conditions used for the measurement, (e.g., the frequency and other experimental parameters).[25] For ZnO in particular this value appears to vary with morphology as well as with post-growth heat treatment.

In order to further confirm charge transfer between $BiVO_4$ and ZnO in the heterojunction material, photoluminescence (PL) spectra were also recorded using a micro Raman laser (Figure 2b). The PL spectrum for bare $BiVO_4$ displays an intense, broad peak at ca. 550 nm. The insert figure displays the PL spectrum of bare ZnO nanorods, with the broad peak centering at ≈580 nm corresponding to defect emissions or oxygen vacancies.[33,34] It is obvious that the spectrum of 1D $BiVO_4$/ZnO heterojunction is broader, which can be fitted into two components. One is due to the luminescence of $BiVO_4$ and the other related to ZnO. The PL peak centered at 560 nm exhibits a near 50% decrease in intensity with respect to pure $BiVO_4$ even if the 1D $BiVO_4$/ZnO heterojunction represents a stronger optical absorption than pure $BiVO_4$ film. The obvious quenching of luminescence of $BiVO_4$ (approximately two times) is characteristic of charge transfer between the $BiVO_4$ and ZnO, indicating that an efficient reduction in recombination of charge carriers in the 1D heterojunction material is taking place.

Following the indication by PL measurement and in order to observe the charge separation function of the single junction, the anodic current–voltage (*I–V*) performance was monitored for a 300 nm thick $BiVO_4$/900 nm ZnO heterojunction electrode measured under visible light irradiation ($\lambda > 420$ nm) in a 0.2 M Na_2SO_4 electrolyte (pH 6.5) in which $BiVO_4$ is the only material absorbing photons as illustrated in Figure 1b. Photocurrent in the dark and for bare $BiVO_4$ and bare ZnO is also plotted under identical condition. All results are shown in **Figure 3**a. The photocurrent for bare $BiVO_4$ increased steadily upon increasing the potential of the working electrode and a photocurrent of ≈0.25 mA cm^{-2} (1.2 V vs RHE) was obtained for a 300 nm thick $BiVO_4$ film. The 900 nm thick ZnO sample exhibited virtually zero photocurrent under visible irradiation due to its large band-gap. Surprisingly the 1D $BiVO_4$/ZnO

electrode for the first time under visible irradiation exhibits a steady photocurrent of ≈2 mA cm^{-2} at 1.2 V (vs RHE). It is nearly 8 times the photocurrent of the pure $BiVO_4$ film. The onset voltage also cathodically shifts from 0.6 V to approximately 0.2 V (vs RHE) compared to the pure $BiVO_4$. All these results promise a large pure energy output. The 8-fold increase in photocurrent compared to the sum of bare $BiVO_4$ and ZnO is only attributed to the enhanced visible absorption and charge separation by $BiVO_4$ and ZnO junction because there is no absorption by ZnO. Compared with the onset voltage of the similar metal oxide junction very recently reported, e.g., between $BiVO_4$ and WO_3 (0.1 V vs Ag/AgCl, pH 6.6),[14] which is similar to the pure $BiVO_4$ in the study, the onset voltage of the ordered $BiVO_4$/ZnO junction is 0.4 V smaller. A good performance in the low potential region is critical for widening the operating window and therefore achieving a high solar to fuel conversion efficiency. In order to assess the poor catalytic activity for water oxidation of $BiVO_4$ and confirm efficient charge transfer from $BiVO_4$ to ZnO, current–voltage curves for $BiVO_4$ and $BiVO_4$/ZnO were recorded in the presence of an efficient sacrificial electron donor in the form of sulphite ions (0.1 M Na_2SO_3) under visible light irradiation (Supporting Information Figure S3). Oxidation of sulphite is kinetically and thermodynamically more favourable than water oxidation;[19] the photocurrent for $BiVO_4$ generated in the presence of sulphite ions increases dramatically to ≈1.25 mA cm^{-2} at 1 V vs RHE, nearly 5 times higher than that of $BiVO_4$ in the identical electrolyte. However the photocurrent of $BiVO_4$/ZnO junction increased only slightly (less than 10%) in the presence of sulphite at the same potential, which clearly indicates that the surface states in conjunction with recombination of charge carriers (due to low electron mobility)[21] are major limiting factors for photocurrent generation in $BiVO_4$ and the novel junction has a similar function to a hole scavenger, leading to efficient in situ electron-hole separation.

The photocurrent of the novel junction was also measured under under full arc AM 1.5G illumination as a reference (Supporting Information Figure S4). Furthermore, under similar experimental conditions the value of 1.75 mA cm^{-2} at 1 V (vs RHE) is much larger in comparison to the recently reported $BiVO_4$/WO_3 junction (≈1 mA cm^{-2} at 1 V vs RHE).[14] The film thickness was optimized and the results for both bare $BiVO_4$ and heterojunction $BiVO_4$/ZnO electrodes with a 900 nm ZnO layer under full arc AM 1.5G illumination are summarized in Table S1, Supporting Information. It is noteworthy however, that upon increasing the thickness of the $BiVO_4$ layer the maximum measured photocurrent decreases, most probably due to comparatively longer charge carrier diffusion lengths in the thicker samples, which would increase the likelihood of recombination in the $BiVO_4$ layer. The stability of a photoelectrode is one of the key factors for its practical application and the $BiVO_4$/ZnO stability was thus tested. It was recorded using the same three electrode cell (1 V vs RHE) for heterojunction $BiVO_4$/ZnO and is shown in **Figure 4**. The light irradiation onto the photoelectrode was controlled using a mechanical chopper. Extremely good stability has been observed throughout the time frame with no apparent loss in current throughout the 180 min time period. $BiVO_4$ was less stable, with some gradual decrease over the time course, which resulted in 84% residual

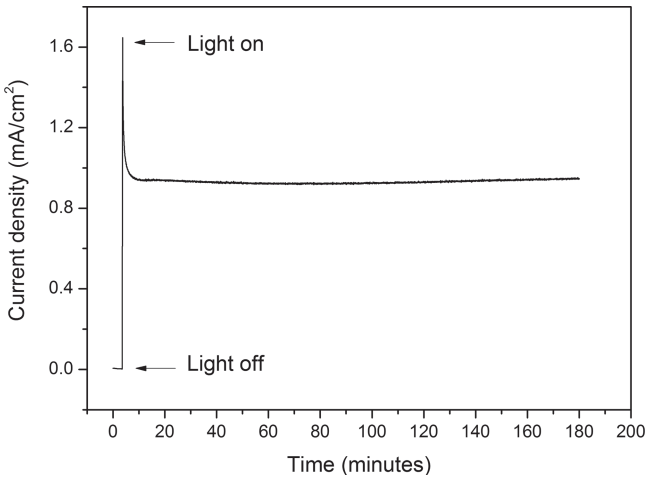

Figure 4. Photocurrent stability measurement of a $BiVO_4$/ZnO bi-junction photoelectrode at an applied potential of 1 V (vs RHE).

photocurrent even after 20 min measurement, in agreement with previous reports that bare $BiVO_4$ has limited stability.[18,32] No change in the $BiVO_4$/ZnO electrode was observed through SEM and XRD patterns recorded after the stability measurement (see Supporting Information Figure S5), inferring that the junction is stable under the present experimental condition. The reason for the relatively enhanced stability is very likely due to efficient charge separation and transport, which prevents the photocorrosion of the photoanode, similar to $BiVO_4$ coupled with FeOOH,[18] the detailed reason for which is currently being investigated.

Incident photon to current efficiency (IPCE) was measured in order to ascertain the light conversion efficiency of heterojunction $BiVO_4$/ZnO and compared to a bare $BiVO_4$ electrode and ZnO in Figure 3b. The IPCE of bare $BiVO_4$ is comparatively low at ≈4% at 410 nm, similar to other studies reporting films of similar thicknesses,[35] whereas heterojunction $BiVO_4$/ZnO is significantly higher at nearly 40% at 410 nm, nearly four times higher than the IPCE of bare $BiVO_4$. This again suggests that the rectifying electron transfer from $BiVO_4$ to ZnO likely inhibits fast recombination and increases the solar energy conversion efficiency of the junction. The IPCE is nearly zero at 550 nm, which is consistent with the sample's optical absorption. Furthermore, a cobalt phosphate (Co-Pi) layer was introduced via photoassisted electrodeposition[36] onto the 300 nm $BiVO_4$/900 nm ZnO electrode to form a junction cascade. Its optical absorption is shown in Figure 1b, exhibiting a similar band-gap absorption to the $BiVO_4$/ZnO junction. Interestingly, a marked improvement in photocurrent has been observed, (≈3 mA cm^{-2} at 1.2 V vs RHE, **Figure 5**a), compared with 1.8 mA cm^{-2} ($BiVO_4$/ZnO) and 0.3 mA cm^{-2} ($BiVO_4$) at 1.2 V vs RHE (Supporting Information Figure S4). It is also higher than the recorded photocurrent of modified $BiVO_4$ heterojunction electrodes recently reported (less than 2.5 mA cm^{-2} at 1.2 V vs RHE),[14,15] and similar to that recorded for the benchmark Co-Pi/W:$BiVO_4$ junction recently reported (≈3 mA cm^{-2} at 1.2 V vs RHE, TEC 15 substrate).[20] IPCE of the triple junction was also measured (Figure 5b), revealing an 18% increase in efficiency (≈47% at 410 nm) compared to $BiVO_4$/ZnO described earlier.

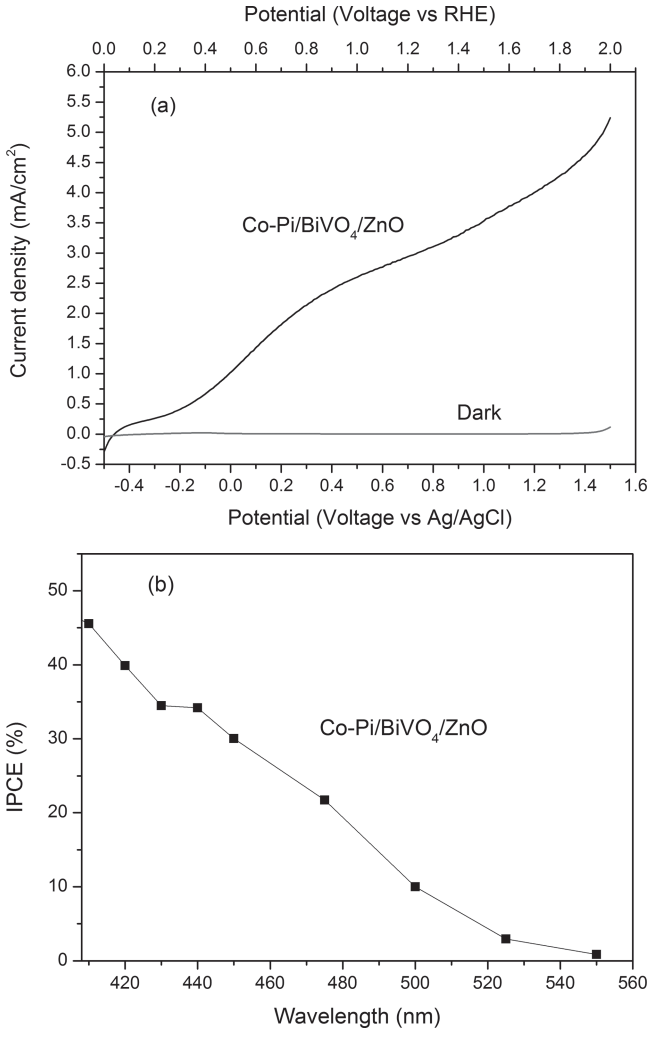

Figure 5. a) Current vs potential curves of Co-Pi/$BiVO_4$/ZnO heterojunction film in a 0.2 M Na_2SO_4 solution (pH 6.5) together with dark current. b) IPCE spectra for Co-Pi modified $BiVO_4$/ZnO bi-junction photoelectrode measured at 1.2 V vs RHE.

Photoassisted electrodeposition of Co-Pi is able to create an adequate junction onto $BiVO_4$, which improves the kinetics for water oxidation, through its function is as a surface electrocatalyst. Stable Co-Pi modified W-$BiVO_4$ electrodes have been demonstrated to cathodically shift the onset potential of $BiVO_4$ for water oxidation and almost completely suppress surface recombination.[37] The "triple" junction Co-Pi/$BiVO_4$/ZnO thus facilitates efficient hole transfer and water oxidation directly on the surface of Co-Pi/$BiVO_4$, while electrons are effectively channeled via ZnO rods to the counter electrode.

The stability of the Co-Pi modified $BiVO_4$/ZnO electrode was examined (Supporting Information Figure S6) and found that the photocurrent decreases a little after 3 hours. The stability enhancement by increasing the adhesion of Co-Pi on $BiVO_4$/ZnO is underway. The solar energy conversion efficiency, η, was estimated to be 0.88% using the current obtained from the stability test (Supporting Information Figure S6) using a potential of 0.5 V (vs Ag/AgCl) for the Co-Pi/$BiVO_4$/ZnO electrode, which demonstrates an order of magnitude increase in comparison to the other very recently reported for CoO/$BiVO_4$ particle p-n junction photoelectrodes operated under the relatively similar condition (0.6 V vs Ag/AgCl electrode at pH 6.9)[16] and double that obtained for Co-Pi modified W:$BiVO_4$ (0.4% at 0.72 V vs RHE).[37]

Charge generation, transfer and transport in 1D $BiVO_4$/ZnO photoanodes is proposed using the results obtained from Mott-Schottky measurements and PL spectra, that revealed a flat-band position of +0.05 V and +0.25 V vs RHE for $BiVO_4$ and ZnO respectively. The difference between the flat-band and conduction band for an oxide semiconductor approximates to 0.3 V,[38,39] thus the conduction band vs NHE at pH 0 is –0.25 V for $BiVO_4$ and –0.05 V for ZnO nanorods, respectively. On the other hand, the addition of Co-Pi (hole acceptor) further facilitates charge separation and water oxidation. The mechanism for the increase in measured photocurrent and efficiency is as follows: upon excitation by visible light, electrons are photoexcited from the valence band of $BiVO_4$ to its conduction band, followed by rectifying transfer to the ordered ZnO nanorods, then fast transport via the rod structure to the conductive substrate, finally to the Pt counter electrode via the external circuit where proton reduction to H_2 could occur. Meanwhile, facile hole migration to Co-Pi on the surface of $BiVO_4$ for water oxidation is promoted. Therefore the light trapping effect, the high conductivity and electron mobility in the ordered ZnO nanorods and the catalytic effect of Co-Pi play very important roles in increasing solar energy conversion efficiency apart from the in situ rectifying charge separation by the bi-junction structure.[40]

3. Conclusions

Overall, a novel material strategy has been proposed:- the highly ordered 1D Co-Pi/$BiVO_4$/ZnO triple junction for photoelectrochemical water splitting. Firstly, a high, steady photocurrent of ≈2 mA cm^{-2} at 1.2 V (vs RHE) and a small onset potential of ≈0.2 V have been achieved for the 1D $BiVO_4$/ZnO junction photoelectrode under visible light irradiation (λ > 420 nm). An IPCE was measured that is almost eight times higher than that of the bare $BiVO_4$ at 410 nm. By the addition of Co-Pi on the $BiVO_4$/ZnO junction surface, an ordered triple junction has been achieved, leading to an extremely high photocurrent of ≈3 mA cm^{-2} measured at 1.2 V vs RHE, which is nearly 12 times and 1.5 times the photocurrent achieved by $BiVO_4$ single photoelectrode and $BiVO_4$/ZnO bi-junction, respectively. Furthermore, it has been demonstrated for the first time, a high energy conversion efficiency of ≈0.88% for $BiVO_4$-based junction photoelectrode without the need of any scavengers. Photoluminescence spectra revealed emission quenching due to matching ZnO rods to $BiVO_4$ nanoparticles, together with flat-band measurements, indicative of efficient charge transfer and separation. This ordered Co-Pi/$BiVO_4$/ZnO junction cascade represents a simple but significant step in improving the solar energy conversion efficiency in $BiVO_4$ by effectively addressing the three limiting factors described in our introduction. Straightforward structural optimization could lead to a further improvement in efficiency, such as optimizing the length and diameter of the ZnO nanorods which will allow for more $BiVO_4$ to be coated

on the ZnO nanorods and furthermore, the selection of different low-cost co-catalysts which can speed up both water reduction and oxidation reactions. In addition, this material design strategy could also be used for other photocatalysts and solar cells where recombination and charge transport dominate energy conversion efficiency.

4. Experimental Section

Film Growth: Films of $BiVO_4$ were deposited onto FTO coated glass substrates (TEC 15, 35 Ω, Pilkington NSG) via a spray pyrolysis method. A 0.02 M solution of bismuth nitrate pentahydrate [$Bi(NO_3)_3.5H_2O$] (Sigma, 99.9%) and [$VO(acac)_2$] (Fisher, 99%) were dissolved in 2-methoxyethanol (Sigma, 99.9%) and sprayed directly onto the FTO glass at a temperature of 200 °C at a distance of 20 cm. The number of spray repetitions determined the overall film thickness; for a thickness of 300 nm approximately 220 spray repetitions were required using a 2 cm^2 spray nozzle. Films were subsequently annealed in air in a muffle furnace at 450 °C for 3 h. Prior to growth of ZnO nanorods, the FTO glass substrates were covered with three layers of ZnO seed crystals deposited via spray pyrolysis (same apparatus as above) from a 0.005 M zinc acetate-ethanol solution followed by heat treatment in air at 350 °C for 30 min. During spray treatment the substrate was kept at ambient temperature and the process carried out at least three times to obtain a conformal covering of ZnO seeds. 1D ZnO nanorod films were grown via an aqueous hydrolysis and condensation procedure[27] using 0.025 M aqueous solutions of zinc nitrate hexahydrate [$Zn(NO_3)_2.6H_2O$] and hexamethylenetetramine (HMT) onto the ZnO seed layer. ZnO nanorod films were grown using a water bath set at 90 °C for 4 h. Films were washed with cold deionized water to remove excess HMT and unreacted or non-adherent particles. Heterojunction $BiVO_4$/ZnO electrodes were produced by spraying the bismuth-vanadium solution directly onto a ZnO nanorod film at 200 °C, followed by annealing in air at 450 °C for 3 h. Photoassisted electrodeposition of cobalt phosphate (Co-Pi) was carried out by the procedure previously reported using a three electrode cell (0.4 V vs Ag/AgCl, Pt counter electrode)[36] through immersion of the photoelectrodes in 0.5 mM cobalt nitrate in 0.1 M phosphate buffer at pH 7 under AM1.5 G illumination. The deposition time was 1500 s.

Film Characterization: The crystallographic phase(s) of these as-prepared products were determined by powder XRD in reflection geometry (Bruker D4, Cu$K\alpha$ radiation source, λ = 1.54054 Å). The morphologies of the samples were observed by SEM, (JSM-7401F, JEOL, 3 kV). The UV-vis absorption spectra were recorded using a UV-vis spectrophotometer equipped with an integrating sphere device (UV-2550, Shimadzu) at room temperature. Raman spectra were acquired using a Renishaw micro-Raman 1000 machine using either 325 nm (PL) or 442 nm (Raman) lasers at room temperature.

Photoelectrochemical Measurements: These were carried out using an Iviumstat potentiostat and associated Ivium software. A three electrode setup was utilized within a Pyrex glass cell sealed with a rubber stopper. A Pt wire mesh and Ag/AgCl electrode were used as the counter and reference electrodes, respectively. An aqueous solution of 0.2 M Na_2SO_4, (with and without the addition of 0.1 M Na_2SO_3) was used as the electrolyte (pH 6.5) and was purged with argon gas for 15 min prior to use to remove any dissolved oxygen. The light source was a 150 W xenon lamp (Newport, USA) equipped with a standard AM 1.5G filter; the light intensity was measured using a silicon photodiode and a Newport hand-held Optical Meter (Model 1918-R). Visible light experiments were conducted using a long-pass filter (λ > 420 nm, Newport). The scan rate was 10 mV s^{-1} and the scanned range was –0.5 to +1.5 V (vs Ag/AgCl). The potential was converted to RHE (reference hydrogen electrode) potentials using E(RHE) =E(Ag/AgCl) + (0.059 × pH) + 0.197 V. Stability measurements (current-time) were conducted using an in-house built mechanical chopper. IPCE was measured with the aid of a monochromator, and calculated using the following equation:

$$\text{IPCE}(\%) = [1240 \times \text{photocurrent density}]/[\text{wavelength} \times \text{photon flux}] \times 100\%$$

The solar energy conversion efficiency (η) was estimated using the following equation:[16]

$$\eta(\%) = [\text{photocurrent density} \times (1.23 - E_{appl})] / [\text{light intensity(AM 1.5G)}] \times 100\%$$

The semiconductor electrodes were irradiated through the FTO glass. Mott-Schottky (Impedance) measurements were measured in 0.2 M Na_2SO_4 in the dark at a frequency of 960 Hz (1 KHz) and scan rate of 10 mV s^{-1}. The potential was measured against an Ag/AgCl reference electrode.

Supporting Information

Supporting Information is available from the Wiley Online Library or from the author.

Acknowledgements

The authors thank the EPSRC for financial support. Mr. Yimeng Ma and Prof. James Durrant (Imperial College) are thanked for useful discussions.

Received: October 18, 2013
Revised: February 17, 2014
Published online: March 20, 2014

[1] A. Bard, M. Fox, *Acc. Chem. Res.* **1995**, *28*, 141.
[2] J. Tang, J. R. Durrant, D. R. Klug, *J. Am. Chem. Soc.* **2008**, *130*, 13885.
[3] K. Li, D. Martin, J. Tang, *Chinese J. Catal.* **2011**, *32*, 879.
[4] A. Kudo, Y. Miseki, *Chem. Soc. Rev.* **2009**, *38*, 253.
[5] K. Sivula, R. Zboril, F. Le Formal, R. Robert, A. Weidenkaff, J. Tucek, J. Frydrych, M. Grätzel, *J. Am. Chem. Soc.* **2010**, *132*, 7436.
[6] G. Hodes, D. Cahen, J. Manassen, *Nature* **1976**, *260*, 312.
[7] C. A. Bignozzi, S. Caramori, V. Cristino, R. Argazzi, L. Meda, A. Tacca, *Chem. Soc. Rev.* **2013**, *42*, 2228.
[8] K. Sayama, A. Nomura, Z. Zou, R. Abe, Y. Abe, H. Arakawa, *Chem. Commun.* **2003**, 2908.
[9] R. Li, F. Zhang, D. Wang, J. Yang, M. Li, J. Zhu, X. Zhou, H. Han, C. Li, *Nat. Commun.* **2013**, *4*, 1432.
[10] Y.-J. Lee, D. S. Ruby, D. W. Peters, B. B. McKenzie, J. W. P. Hsu, *Nano Lett.* **2008**, *8*, 1501.
[11] X. Cao, P. Chen, Y. Guo, *J. Phys. Chem. C* **2008**, *112*, 20560.
[12] A. Kudo, K. Omori, H. Kato, *J. Am. Chem. Soc.* **1999**, *121*, 11459.
[13] Y. Park, K. J. McDonald, K.-S. Choi, *Chem. Soc. Rev.* **2012**, *42*, 2321.
[14] S. J. Hong, S. Lee, J. S. Jang, J. S. Lee, *Energy Environ. Sci.* **2011**, *4*, 1781.
[15] R. Saito, Y. Miseki, K. Sayama, *Chem. Commun.* **2012**, *48*, 3833.
[16] Q. Jia, K. Iwashina, A. Kudo, *Proc. Natl. Acad. Sci.* **2012**, *109*, 11564.
[17] F. Abdi, R. van de Krol, *J. Phys. Chem. C* **2012**, *116*, 9398.
[18] J. A. Seabold, K.-S. Choi, *J. Am. Chem. Soc.* **2012**, *134*, 2186.
[19] K. J. McDonald, K.-S. Choi, *Energy Environ. Sci.* **2012**, *5*, 8553.
[20] F. F. Abdi, L. Han, A. H. M. Smets, M. Zeman, B. Dam, R. van de Krol, *Nat. Commun.* **2013**, *4*, 2195.
[21] F. F. Abdi, T. J. Savenije, M. M. May, B. Dam, R. Van De Krol, *J. Phys. Chem. Lett.* **2013**, *4*, 2752.
[22] M. Long, W. Cai, H. Kisch, *J. Phys. Chem. C* **2008**, *112*, 548.

[23] K. Sayama, A. Nomura, T. Arai, T. Sugita, R. Abe, M. Yanagida, T. Oi, Y. Iwasaki, Y. Abe, H. Sugihara, *J. Phys. Chem. B* **2006**, *110*, 11352.
[24] S. Berglund, D. Flaherty, *J. Phys. Chem. C* **2011**, *115*, 3794.
[25] A. Wolcott, W. A. Smith, T. R. Kuykendall, Y. Zhao, J. Z. Zhang, *Adv. Funct. Mater.* **2009**, *19*, 1849.
[26] M. Law, L. E. Greene, J. C. Johnson, R. Saykally, P. Yang, *Nat. Mater.* **2005**, *4*, 455.
[27] L. E. Greene, M. Law, D. H. Tan, M. Montano, J. Goldberger, G. Somorjai, P. Yang, *Nano Lett.* **2005**, *5*, 1231.
[28] L. E. Greene, M. Law, J. Goldberger, F. Kim, J. C. Johnson, Y. Zhang, R. J. Saykally, P. Yang, *Angew. Chem. Int. Ed.* **2003**, *42*, 3031.
[29] D. Pradhan, S. K. Mohapatra, S. Tymen, M. Misra, K. T. Leung, *Mater. Express* **2011**, *1*, 59.
[30] D. Polsongkram, P. Chamninok, S. Pukird, L. Chow, O. Lupan, G. Chai, H. Khallaf, S. Park, A. Schulte, *Physica B* **2008**, *403*, 3713.
[31] R. L. Frost, D. A. Henry, M. L. Weier, W. Martens, *J. Raman Spectrosc.* **2006**, *37*, 722.
[32] W. Luo, Z. Yang, Z. Li, J. Zhang, J. Liu, Z. Zhao, Z. Wang, S. Yan, T. Yu, Z. Zou, *Energy Environ. Sci.* **2011**, *4*, 4046.
[33] A. B. Djurisi , Y. H. Leung, *Small* **2006**, *2*, 944.
[34] W. I. Park, D. H. Kim, S.-W. Jung, G.-C. Yi, *Appl. Phys. Lett.* **2002**, *80*, 4232.
[35] X. Yang, A. Wolcott, G. Wang, A. Sobo, R. C. Fitzmorris, F. Qian, J. Z. Zhang, Y. Li, *Nano Lett.* **2009**, *9*, 2331.
[36] D. K. Zhong, M. Cornuz, K. Sivula, M. Grätzel, D. R. Gamelin, *Energy Environ. Sci.* **2011**, *4*, 1759.
[37] D. K. Zhong, S. Choi, D. R. Gamelin, *J. Am. Chem. Soc.* **2011**, *133*, 18370.
[38] Y. Matsumoto, *J. Solid State Chem.* **1996**, *126*, 227.
[39] W. Chun, A. Ishikawa, H. Fujisawa, T. Takata, J. Kondo, M. Hara, M. Kawai, Y. Matsumoto, K. Domen, *J. Phys. Chem. B* **2003**, *107*, 1798.
[40] Y. F. Hsu, Y. Y. Xi, A. B. Djurisic , W. K. Chan, *Appl. Phys. Lett.* **2008**, *92*, 133507.